RESEARCH ARTICLE

MAC3A and MAC3B mediate degradation of the transcription factor ERF13 and thus promote lateral root emergence

Zipeng Yu[1†], Xingzhen Qu[1†], Bingsheng Lv[2], Xiaoxuan Li[1], Jiaxuan Sui[1], Qianqian Yu[3], and Zhaojun Ding[1*]

[1] The Key Laboratory of Plant Development and Environmental Adaptation Biology, Ministry of Education, School of Life Sciences, Shandong University, Qingdao, Shandong, 266237, China.

[2] College of Horticulture, Qingdao Agricultural University, Qingdao, Shandong 266109, China.

[3] School of Life Sciences, Liaocheng University, Liaocheng, Shandong, 252000, China.

[†] These authors contributed equally to this work

Short Title: MAC3A and MAC3B promote lateral root emergence

* Corresponding author: Zhaojun Ding (dingzhaojun@sdu.edu.cn)

The author responsible for distribution of materials integral to the findings presented in this article in accordance with the policy described in the Instructions for Authors (https://academic.oup.com/plcell/pages/General-Instructions) is: Zhaojun Ding (dingzhaojun@sdu.edu.cn).

Abstract

Lateral roots (LRs) increase root surface area and allow plants greater access to soil water and nutrients. LR formation is tightly regulated by the phytohormone auxin. Whereas the transcription factor ETHYLENE-RESPONSIVE ELEMENT BINDING FACTOR13 (ERF13) prevents LR emergence in Arabidopsis (*Arabidopsis thaliana*), auxin activates MITOGEN-ACTIVATED PROTEIN KINASE14 (MPK14), which leads to ERF13 degradation and ultimately promotes LR emergence. In this study, we discovered interactions between ERF13 and the E3 ubiquitin ligases MOS4-ASSOCIATED COMPLEX 3A (MAC3A) and MAC3B. As MAC3A and MAC3B gradually accumulate in the LR primordium, ERF13 levels gradually decrease. We demonstrate that MAC3A and MAC3B ubiquitinate ERF13, leading to its degradation and accelerating the transition of LR primordia from stage IV to stage V. Auxin enhances the MAC3A and MAC3B interaction with ERF13 by facilitating MPK14-mediated ERF13 phosphorylation. In summary, this study reveals the molecular mechanism by which auxin eliminates the inhibitory factor ERF13 through the MPK14–MAC3A and MAC3B signaling module, thus promoting LR emergence.

Keywords: Auxin; Lateral root emergence; ERF13; MAC3A and MAC3B; MPK14.

Introduction

Plants have evolved flexible root systems that enable them to adapt to the heterogeneous distribution of water and nutrients in the soil (Karlova et al., 2021). Lateral root (LR) formation and elongation are key features of this root plasticity, and both processes are tightly regulated by the phytohormone auxin. The localized accumulation of auxin in root pericycle cells serves as a morphogenetic signal, determining their fate as lateral root founder cells, which give rise to the lateral root primordia (LRP) that eventually generate visible LRs (Banda et al., 2019). LRP formation encompasses eight distinct stages, including stages I–IV in the endodermis, stages V and VI in the cortex, stage VII in the epidermis, and stage VIII, in which the LRP breaks through the epidermis (Malamy and Benfey, 1997).

Auxin influences all aspects of LR formation, from initiation to emergence (Banda et al., 2019). AUXIN RESPONSE FACTOR7 (ARF7) and ARF19 mediate auxin signaling during LRP development in Arabidopsis (*Arabidopsis thaliana*) via the transcriptional regulation of different downstream targets. Among these targets, LATERAL ORGAN BOUNDARIES DOMAIN (LBD) proteins promote LR formation, mainly through the transcriptional regulation of *EXPANSIN* genes and cell wall remodeling during LR emergence (Banda et al., 2019). Additionally, MITOGEN-ACTIVATED PROTEIN KINASE (MPK) family members MPK3 and MPK6 are activated by auxin, influencing LR formation by regulating cell division patterns and cell wall remodeling processes (Huang et al., 2019; Zhu et al., 2019). A role for MPK14 in auxin-induced LR formation has also been reported: activation of MPK14 by auxin leads to the degradation of ETHYLENE-RESPONSIVE ELEMENT BINDING FACTOR13 (ERF13), an inhibitory protein that restricts LRP development during the transition from stage IV to stage V (Lv et al., 2021). However, the players that mediate ERF13 degradation during LR formation remain elusive.

The U-box-type E3 ubiquitin ligase MOS4-ASSOCIATED COMPLEX 3A [MAC3A, also known as PLANT U-BOX59 (PUB59)] and its homolog MAC3B (also known as PUB60) were first identified as the core components of the MOS4-ASSOCIATED COMPLEX (MAC) involved in plant innate immunity (Monaghan et al., 2009). MAC3A and MAC3B promote microRNA biogenesis, together with the other core MAC subunits CELL DIVISION CYCLE5 (CDC5/MAC1), PLEIOTROPIC REGULATORY LOCUS1 (PRL1/MAC2), and MAC7 (Jia et

al., 2017; Li et al., 2018). In addition, MAC3A and MAC3B maintain the circadian clock by facilitating the proper splicing of clock-related genes (Feke et al., 2019) and regulate flowering time by degrading a currently unknown target protein (Feke et al., 2020). MAC3A and MAC3B were recently proposed to be determinants of seed longevity (Ninoles et al., 2022), which may be related to their regulation of abscisic acid-mediated alternative splicing (Tu et al., 2022). In addition to regulating plant growth and development, MAC3A and MAC3B also play essential roles in environmental fitness, especially adaptation to salt stress, which mainly depends on the correct splicing of salt tolerance-related genes (Li et al., 2019). In summary, MAC3A and MAC3B regulate splicing in a MAC-dependent manner. Notably, although MAC3A and MAC3B exhibited E3 ligase activity *in vitro* in a MAC-independent manner (Wiborg et al., 2008; Li et al., 2018), to date, no direct targets that are ubiquitinated by MAC3A and MAC3B have been reported.

To identify which ubiquitin ligase is responsible for clearing of ERF13 protein during LR emergence, we did immunoprecipitation-mass spectrometry assays. Our findings revealed the interaction between ERF13 and the E3 ubiquitin ligases MAC3A and MAC3B and demonstrate the essential roles of MAC3A and MAC3B in auxin-induced ERF13 degradation and subsequent LR emergence in Arabidopsis. We demonstrate that MAC3A and MAC3B preferentially recognize and ubiquitinate the phosphorylated form of ERF13, which is facilitated by MPK14. We propose that auxin-activated MPK14 phosphorylates ERF13, prompting its recruitment of MAC3A and MAC3B and the resulting degradation of ERF13 at the LRP, leading to LR emergence.

Results

ERF13 interacts with the ubiquitin ligases MAC3A and MAC3B

We previously showed that the barrier protein ERF13 prevents LR emergence under low auxin concentrations and that high auxin concentrations induce ERF13 degradation, leading to LR emergence (Lv et al., 2021). To investigate the mechanism by which auxin triggers ERF13 degradation, we aimed to identify ERF13-interacting proteins, with a particular emphasis on finding ubiquitin ligases. We performed immunoprecipitation-mass spectrometry (IP-MS) of transgenic *Pro35S:ERF13-MYC* Arabidopsis seedlings. Among the 84 candidate ERF13-

interacting proteins (Supplemental Table S1), we focused on the ubiquitin ligase MAC3B, along with its homologous protein MAC3A, which share 82% protein sequence similarity (Monaghan et al., 2009). We confirmed the interaction of ERF13 with MAC3A and MAC3B via co-immunoprecipitation (Co-IP) experiments in Arabidopsis protoplasts and luciferase complementation imaging (LCI) assays in *Nicotiana benthamiana* leaves (Figure 1, A and B).

MAC3A and MAC3B are members of the U-box-type E3 ligase family, with the U-box domain facilitating the recruitment of E2 ubiquitin-conjugating enzymes for target protein degradation (Feke et al., 2019). Notably, LCI assays showed that ERF13 exhibited stronger interactions with MAC3A$^{\Delta U\text{-box}}$ and MAC3B$^{\Delta U\text{-box}}$ (lacking the U-box domain) compared to full-length MAC3A and MAC3B (Figure 1C), pointing to the potential involvement of full-length MAC3A and MAC3B in ERF13 degradation. As expected, treatment with the 26S proteasome inhibitor MG132 substantially enhanced the interactions between ERF13 and full-length MAC3A and MAC3B in LCI assays (Supplemental Figure S1). In addition, bimolecular fluorescence complementation (BiFC) experiments in *N. benthamiana* leaves revealed that ERF13 interacts with MAC3A$^{\Delta U\text{-box}}$ and MAC3B$^{\Delta U\text{-box}}$ in the nucleus (Figure 1D), which is consistent with our recent finding on the nuclear localization of ERF13 (Lv et al., 2021).

MAC3A and MAC3B play an important role in LR emergence

Given the role of ERF13 in restricting LR emergence (Lv et al., 2021), we investigated whether MAC3A and MAC3B accumulate in LRP and contribute to LR emergence. Histochemical β-glucuronidase (GUS) staining of *ProMAC3A:GUS* and *ProMAC3B:GUS* seedlings revealed that *MAC3A* and *MAC3B* were ubiquitously expressed in various plant tissues, including young leaves, primary root tips, stele, and LRP at all stages of development (Figure 2A). We also examined *MAC3A* expression in *ProMAC3A:MAC3A-GFP/mac3a mac3b* plants. MAC3A-GFP was expressed at various stages of LRP development and localized to the nucleus in cells of both lateral and primary roots (Figure 2B and Supplemental Figure S2), which is consistent with the nuclear localization of MAC3A in guard cells (Monaghan et al., 2009).

To investigate the roles of MAC3A and MAC3B in LR development, we analyzed the phenotypes of the LRs of *mac3a-1* (Salk_143098), *mac3a-2* (Salk_089300), and *mac3b-2* (Salk_144856) single mutants (Supplemental Figure S3) and the *mac3a mac3b* double mutant

obtained by crossing *mac3a-2* with *mac3b* (Salk_050811) (Li et al., 2018). The single mutants showed comparable LR densities to the wild type (WT), whereas the *mac3a mac3b* double mutant exhibited a significant reduction in total LR density and emerged lateral root (LRE) density compared to WT (Figure 2, C and D). These results suggest that *MAC3A* and *MAC3B* redundantly and positively regulate LR emergence.

Additionally, introducing *ProMAC3A:MAC3A-GFP* into *mac3a mac3b* rescued the root development phenotypes of the mutant, including reduced LR density and shorter primary roots (Figure 2, C and D and Supplemental Figure S4). These results suggest that MAC3A and MAC3B are also important regulators of primary root development in addition to their roles in LR development. Furthermore, we investigated the role of MAC3A and MAC3B in auxin-promoted LR formation by treating Arabidopsis seedlings with the synthetic auxin analog naphthaleneacetic acid (NAA). Auxin-induced LR formation was weakened in the *mac3a mac3b* mutant compared to the WT control (Supplemental Figure S5), indicating that MAC3A and MAC3B function in auxin-regulated LR formation.

MAC3A and MAC3B counteract the inhibitory effect of ERF13 on LR development

LRP development was blocked at stage IV in the *mac3a mac3b* mutant, resulting in an increased frequency of stage IV LRP and a decreased frequency of LRP at stages V to VIII (Figure 3, A and B). This phenotypic similarity to *Pro35S:ERF13-MYC* transgenic plants suggests that MAC3A and MAC3B play a role opposite that of ERF13 in promoting the transition of LRP from stage IV to stage V. Introducing *ProMAC3A:MAC3A-GFP* into *mac3a mac3b* rescued the transition of stage IV LRP (Supplemental Figure S6), further supporting the role of MAC3A and MAC3B in this process.

Gravitational stimulation synchronizes LR initiation and facilitates the comparison of LRP development across genotypes (Lucas et al., 2008; Peret et al., 2012). Following 48 hours of gravistimulation, more than 70% of LRP in *mac3a mac3b* seedlings remained at stage IV, which is similar to the observation in *Pro35S:ERF13-MYC* transgenic plants (Figure 3C). Intriguingly, at 18 hours after gravistimulation, we observed an increased frequency of stage I LRP and a reduced frequency of stage II and stage III LRP in *mac3a mac3b* seedlings compared to WT and *Pro35S:ERF13-MYC* seedlings (Supplemental Figure S7). These results suggest

that MAC3A and MAC3B may also play a role in LR initiation, and the *mac3a mac3b* mutant displayed a decelerated LRP development subsequent to their initiation. This may be related to the insufficient expression of *LBD16*, *LBD18*, and *PUCHI* (Supplemental Figure S8), which are key genes for LR initiation (Goh et al., 2012; Goh et al., 2019; Trinh et al., 2019).

ERF13 inhibits LR emergence by suppressing the expression of *3-KETOACYL-COA SYNTHASEs* (*KCSs*) (Lv et al., 2021). Consistent with the antagonistic roles of ERF13 and the E3 ligases MAC3A and MAC3B in LR emergence, we observed a significant reduction in the expression levels of *KCS8*, *KCS16*, and *KCS18* in the *mac3a mac3b* mutant (Figure 3D). While overexpressing *MAC3A* and *MAC3B* in WT seedlings did not promote LR emergence (Supplemental Figure S9), it restored the density of LREs and the expression levels of *KCSs* in *Pro35S:GFP-ERF13* seedlings (Figure 3, E and F and Supplemental Figure S10). These results indicate that MAC3A and MAC3B counteract the inhibitory effect of ERF13 on LR emergence. Furthermore, the mutation of *ERF13* in the *mac3a mac3b* mutant background restored LRE and total LR density to WT levels (Figure 3, G and H), suggesting that ERF13 acts downstream of MAC3A and MAC3B in LR emergence.

MAC3A and MAC3B ubiquitinate and degrade ERF13

Based on GUS staining and analysis of GFP fluorescent signals, although *ERF13* and the E3 ligase encoding genes *MAC3A* and *MAC3B* are transcriptionally expressed in the eight stages of LRP development, they showed opposite patterns at the protein level (Figure 2, A and B and Supplemental Figure S11). As MAC3A gradually accumulated in the LRP, the level of ERF13 gradually decreased. We conducted ubiquitination experiments in Arabidopsis protoplasts to test our hypothesis that MAC3A and MAC3B inhibit ERF13 during LR emergence via E3-mediated ubiquitination and degradation.

We expressed various combinations of ERF13-FLAG, ubiquitin-MYC, and MAC3A-GFP, MAC3B-GFP, or GFP in protoplasts, treated the protoplasts with MG132 to inhibit ERF13 degradation, and performed Co-IP with anti-FLAG antibodies. The results confirmed the interactions between ERF13 and the E3 ligases MAC3A and MAC3B, and importantly, both MAC3A and MAC3B exhibited the ability to ubiquitinate ERF13 (Figure 4A). Subsequently, we introduced ERF13-FLAG, with or without ubiquitin-MYC, into WT and *mac3a mac3b*

protoplasts. We observed the reduced ubiquitination of ERF13-FLAG in *mac3a mac3b* compared to the WT (Figure 4B), indicating that endogenous MAC3A and MAC3B can ubiquitinate ERF13 *in planta*.

Ubiquitination often leads to reduced protein abundance. To further investigate the role of MAC3A and MAC3B in ERF13 abundance, we introduced *Pro35S:MAC3B-MYC* into transgenic *Pro35S:GFP-ERF13* plants and examined the effect of *MAC3B* overexpression on ERF13 protein levels. We observed a notable decrease in the abundance of ERF13 upon *MAC3B* overexpression (Figure 4C and Supplemental Figure S12). Additionally, we conducted a cell-free experiment in which we incubated recombinant GST-ERF13 with total protein extracts from WT, *Pro35S:MAC3B-MYC*, and *mac3a mac3b* seedlings. GST-ERF13 was most stable in total protein extracts lacking MAC3A and MAC3B, with its half-life increasing from 109.5 minutes in WT extracts to 670.0 minutes in *mac3a mac3b* extracts. Conversely, elevated levels of MAC3B significantly shortened the half-life of GST-ERF13 to 41.0 minutes (Figure 4, D and E). These results strongly support the notion that MAC3A and MAC3B promote the ubiquitination and degradation of ERF13.

MAC3A and MAC3B regulate auxin-induced ERF13 degradation

ERF13 represses auxin-induced *KCS16* expression during LR development (Lv et al., 2021). Consistent with the reduced upregulation of *KCS16* after NAA treatment, auxin-promoted LR formation was attenuated in *mac3a mac3b* compared to the WT control (Supplemental Figure S5 and S13), suggesting that MAC3A and MAC3B play a positive role in auxin-induced expression of *KCS16* during LR formation. Based on the finding that ERF13 and the E3 ligases MAC3A and MAC3B play antagonistic roles in auxin-induced LR formation, we reasoned that auxin promotes the MAC3A- and MAC3B-mediated degradation of ERF13. To test this hypothesis, we blocked protein biosynthesis in *Pro35S:GFP-ERF13* and *Pro35S:GFP-ERF13/Pro35S:MAC3B-MYC* seedlings by treating them with cycloheximide (CHX) and subsequently treated them with or without NAA. NAA treatment increased the rate of ERF13 degradation in the WT, and the degradation rate was further enhanced by overexpressing *MAC3B* (Figure 5, A and B). Furthermore, NAA-mediated degradation of ERF13 was notably impaired in *mac3a mac3b* (Figure 5, A and B), suggesting that ERF13 degradation is dependent

on MAC3A and MAC3B.

We investigated whether auxin treatment would enhance the interaction between ERF13 and these E3 ligases by performing Co-IP assays in Arabidopsis protoplasts. We co-expressed *ERF13-MYC* and *MAC3A-GFP* or *MAC3B-GFP* in Arabidopsis protoplasts, treated the protoplasts with NAA in the presence of MG132 to inhibit ERF13 degradation, and examined the co-immunoprecipitation of ERF13-MYC with MAC3A-GFP or MAC3B-GFP. NAA treatment remarkably increased the interaction between ERF13 and these E3 ligases (Figure 5, C and D). Collectively, these findings further support our hypothesis that auxin promotes MAC3A- and MAC3B-mediated degradation of ERF13 by enhancing the interaction between these E3 ligases and ERF13.

MAC3A and MAC3B preferentially interact with and degrade MPK14-phosphorylated ERF13

Auxin-induced ERF13 degradation relies on MPK14-mediated ERF13 phosphorylation at Thr66, Ser67, and Thr124 (Lv et al., 2021). We reasoned that auxin-induced phosphorylation of ERF13 enhances its binding to MAC3A and MAC3B. To test this hypothesis, we generated two variants of ERF13 that mimic the phosphorylated and non-phosphorylated forms. We mutated these residues to aspartic acid (D) in ERF13^{DDD} (phosphomimic) and to alanine (A) in ERF13^{AAA} (cannot be phosphorylated) and verified their interaction with MAC3A and MAC3B through Co-IP experiments. MAC3A-GFP and MAC3B-GFP displayed a slightly weaker interaction with ERF13^{AAA}-MYC compared to ERF13^{WT}-MYC, while it exhibited a much stronger interaction with ERF13^{DDD}-GFP (Figure 6, A and B). This result suggests that phosphorylation of ERF13 enhances its binding to MAC3A and MAC3B, which was further confirmed by ratiometric BiFC (rBiFC) and LCI assays (Figure 6, C and D). Together, these data suggest that MPK14-mediated phosphorylation of ERF13 promotes its interaction with the E3 ligases MAC3A and MAC3B.

Based on the enhanced interaction between ERF13^{DDD} and these E3 ligases, we investigated whether this contributes to the degradation of ERF13 by examining the degradation rates of different phosphorylated forms of ERF13 in WT and *mac3a mac3b* extracts. ERF13^{DDD}, which strongly interacted with MAC3A and MAC3B, underwent rapid

degradation in WT extracts, whereas ERF13^{AAA}, which weakly interacted with MAC3A and MAC3B, remained stable. Furthermore, auxin-induced ERF13 degradation was substantially alleviated in *mac3a mac3b*. Although the degradation of both ERF13^{DDD} and ERF13^{AAA} remained insensitive to NAA treatment, these two versions of ERF13 proteins became particularly stable in *mac3a mac3b* regardless of NAA treatment (Figure 6E). Taken together, these results indicate that auxin promotes the recruitment of the E3 ligases MAC3A and MAC3B via MPK14-mediated phosphorylation of ERF13, leading to ERF13 degradation. The interaction between these E3 ligases and ERF13 appears to be critical for auxin-induced degradation of ERF13 during LR emergence.

Auxin induces MAC3A and MAC3B accumulation in the LRP during LR development

We hypothesized that auxin promotes the interaction between ERF13 and these E3 ligases not only via MPK14-mediated phosphorylation of ERF13 but also by activating MAC3A and MAC3B themselves. Consistent with this hypothesis, NAA treatment led to increased levels of MAC3A-GFP in *ProMAC3A:MAC3A-GFP/mac3a mac3b* seedlings (Figure 7, A and B), suggesting that auxin has a positive effect on these E3 ligases.

We observed increased levels of *MAC3A* and *MAC3B* transcripts after NAA treatment (Figure 7C) and increased histochemical GUS staining in *ProMAC3A:GUS* and *ProMAC3B:GUS* seedlings treated with NAA (Figure 7D), suggesting that auxin positively regulates *MAC3A* and *MAC3B* promoter activity. Auxin-induced LR formation-related genes depend on AUXIN RESPONSE FACTOR (ARF) transcription factors for their activation (Yu et al., 2022). To investigate whether the auxin-induced expression of *MAC3A* and *MAC3B* also relies on ARFs, we examined *MAC3A* and *MAC3B* transcription in *arf7-1* and *arf19-1* in response to NAA treatment. NAA-induced *MAC3A* and *MAC3B* transcription was attenuated in the *arf7-1* and *arf19-1* single mutants and completely abolished in the *arf7-1 arf19-1* double mutant (Figure 7E), suggesting that auxin-induced *MAC3A* and *MAC3B* transcription depends on ARF7 and ARF19.

ARFs typically recognize and bind to auxin-responsive elements (AuxREs) in the promoters of their target genes (Yu et al., 2022). Although the promoters of *MAC3A* and *MAC3B* contain AuxREs (Supplemental Figure S14A), yeast one-hybrid assays did not detect

the direct binding of ARF7 and ARF19 to the *MAC3A* and *MAC3B* promoters (Supplemental Figure S14B). These results suggest that ARF7 and ARF19 indirectly promote *MAC3A* and *MAC3B* transcription.

The strongly enhanced fluorescent signal of MAC3A-GFP under NAA treatment suggested that the role of auxin in positively regulating MAC3A and MAC3B is not limited to the transcriptional level (Figure 7A). To verify this hypothesis, we examined the protein stability of MAC3A and MAC3B in response to auxin and found that NAA treatment markedly enhanced their stability (Supplemental Figure S15). Together, our results suggest that auxin induces the accumulation of MAC3A and MAC3B in the LRP via the synergistic regulation of their transcription and protein stability.

Discussion

In this study, we investigated the molecular mechanism underlying the degradation of ERF13 during auxin-induced LR emergence. Our findings reveal that MAC3A and MAC3B act as E3 ligases that mediate the ubiquitination and degradation of ERF13, providing insight into the complex regulatory network governing auxin-induced LR development. We demonstrated that auxin promotes the interaction between ERF13 and these E3 ligases via two independent mechanisms. First, auxin activates the MPK14-mediated phosphorylation of ERF13, which enhances its binding affinity to MAC3A and MAC3B. Second, auxin promotes MAC3A and MAC3B accumulation at the LRP during LR development. Together, these mechanisms strengthen the interaction between these E3 ligases and ERF13, leading to the ubiquitination and subsequent degradation of ERF13. The degradation of ERF13 releases its inhibitory effect on LR development, enabling the emergence of LR.

We previously reported that ERF13 is a negative regulator of LR emergence and is degraded in response to high auxin concentrations (Lv et al., 2021). Here, we demonstrated that MAC3A and MAC3B positively regulate LR emergence by promoting ERF13 degradation, uncovering the regulation of ERF13 protein levels by MAC3A and MAC3B. Our findings support a model in which auxin-induced phosphorylation of ERF13 and the accumulation of MAC3A and MAC3B synergistically enhance the interaction between these E3 ligases and ERF13, leading to the degradation of ERF13, ultimately resulting in LR emergence (Figure 8).

MAC3A and MAC3B were originally identified as core components of the MAC involved in plant innate immunity (Monaghan et al., 2009). Although MAC3B was shown to be a U-box-type E3 ligase with complete E3 ligase activity when it was first identified (Wiborg et al., 2008), no direct targets that are ubiquitinated by MAC3A and MAC3B have been reported. In the current study, we showed that MAC3A and MAC3B act as E3 ligases to regulate LR emergence via ERF13 degradation. We showed that MAC3A and MAC3B preferentially interact with phosphorylated ERF13 during auxin-induced LR development. MAC is a large complex containing 24 possible subunits (Monaghan et al., 2009), but no subunits besides MAC3B were found to interact with ERF13 (Supplemental Table S1). Thus, our findings indicate that MAC3A- and MAC3B-mediated ERF13 degradation occurs in a MAC-independent manner. This is consistent with the previous finding that MAC3A and MAC3B exhibit E3 ligase activities *in vitro* without the involvement of other MAC subunits (Wiborg et al., 2008; Li et al., 2018). This highlights the specific roles of MAC3A and MAC3B as E3 ligases for ERF13 degradation in the context of LR development.

Our results not only elucidate the role of MAC3A and MAC3B in promoting ERF13 degradation but also reveal their involvement in multiple stages of LR development, including the transition from stage IV to stage V and LR initiation. Considering the importance of PUCHI for the auxin-induced transcription of *KCSs* (Trinh et al., 2019) and the finding that *PUCHI* expression is induced by MAC3A and MAC3B (Supplemental Figure S8C), we hypothesize that auxin upregulates *KCS* gene expression not only by degrading ERF13 but also by inducing PUCHI accumulation. Upregulated *KCSs* ultimately promote the transition of LRP from stage IV to stage V (Lv et al., 2021). The delayed LRP development observed in the *mac3a mac3b* mutant suggests that MAC3A and MAC3B play a key role in regulating LR initiation. Identifying additional targets of MAC3A and MAC3B will provide further insight into the molecular mechanisms underlying their regulation of LR development. In addition, MAC3A- and MAC3B-mediated LRP initiation may be related to the transcription of *LBD16* and *LBD18* (Supplemental Figure S8, D and E). Whether MAC3A and MAC3B are involved in the correct splicing of the mRNA of these genes is also worth exploring.

In conclusion, our study unveils the molecular mechanism by which auxin-induced degradation of ERF13 regulates LR emergence. Our findings highlight the antagonistic roles

of ERF13 and the E3 ligases MAC3A and MAC3B in controlling LR development and provide valuable insight into the complex regulatory network underlying auxin-mediated LR development. Further investigations of the targets and functions of MAC3A and MAC3B will deepen our understanding of their roles in LR development and plant growth in response to environmental conditions.

Materials and Methods

Plant materials and growth conditions

All plant materials used in this study are in the Arabidopsis (*Arabidopsis thaliana*) Columbia-0 (Col-0) background. The *ERF13*-overexpressing lines *Pro35S:GFP-ERF13*#6 and *Pro35S:ERF13-MYC*#6 were described previously (Lv et al., 2021); *Pro35S:MAC3B-MYC* was constructed in this study, and the encoding sequence (CDS) of *MAC3B* was amplified and cloned into the *pGWB18* vector (Zhang et al., 2020); the *Pro35S:GFP-ERF13/Pro35S:MAC3B-MYC* line was generated by crossing *Pro35S:GFP-ERF13* and *Pro35S:MAC3B-MYC* plants; *ProERF13:GUS* was described previously (Lv et al., 2021); *ProMAC3A:GUS* and *ProMAC3B:GUS* were generated in this study, and the promoters of *MAC3A* (3,048 bp upstream of ATG) and *MAC3B* (3,004 bp upstream of ATG) were amplified and cloned into the *pQTY* vector; the T-DNA insertion mutants *mac3a-1* (Salk_143098), *mac3a-2* (Salk_089300), and *mac3b-2* (Salk_144856) were obtained from AraShare (www.arashare.cn/index/Product/index.html); *mac3a mac3b* [*mac3a-2* (Salk_089300); *mac3b* (Salk_050811)], *ProMAC3A:MAC3A-GFP/mac3a mac3b*, and *Pro35S:3MYC-MAC3A/mac3a mac3b* were a gift from Prof. Shengjun Li at the Chinese Academy of Sciences (Li et al., 2018); *ProERF13:ERF13-YFP* was constructed in this study, and the promoter of *ERF13* (2,596 bp upstream of ATG) was amplified with the CDS of *ERF13* and cloned into the *BGW* vector (Shang et al., 2021); *erf13-1* (GK_724B09) was described previously (Lv et al., 2021); *mac3a mac3b erf13-1* was generated by crossing *mac3a mac3b* and *erf13-1*. The following mutants have been described elsewhere: *lbd16* (Okushima et al., 2007); *lbd18* (Fan et al., 2012); *lbd29* (Liu et al., 2010); *lbd16 lbd18 lbd33* (Goh et al., 2012); *puchi-1* (Trinh et al., 2019); *arf7-1*, *arf19-1*, and *arf7-1 arf19-1* (Okushima et al., 2005). *lbd16 lbd18 lbd29* was generated by crossing *lbd16*, *lbd18*, and *lbd29* single mutants. All primers used for the generation and

identification of plant material are listed in Supplemental Table S2. All Arabidopsis and *Nicotiana benthamiana* materials were grown under long-day conditions (16 h light/8 h dark) in a plant growth chamber [PERCIVAL, Thermo Fisher, USA, with 120 μmol m^{-2} s^{-1} (white fluorescent bulbs), and 65% relative humidity] with Arabidopsis at 23°C and *Nicotiana benthamiana* at 26°C.

Protein immunoprecipitation coupled with LC-MS/MS analysis

To identify ERF13-interacting proteins, we performed protein immunoprecipitation (IP) coupled with liquid chromatography–tandem mass spectrometry (LC-MS/MS) using *Pro35S:ERF13-MYC* seedlings. Immunoprecipitation, LC-MS/MS, and data analysis were performed as previously described (Yu et al., 2023). In brief, 8-day-old *Pro35S:ERF13-MYC* seedlings were collected and ground in liquid nitrogen. A 4-g sample was combined with 4 mL lysis solution [1% (v/v) Triton X-100, 150 mM NaCl, a protease inhibitor cocktail tablet, 50 mM Tris-HCl (pH 7.5), and 5 mM EDTA], incubated for 40 min, and centrifuged for 15 min at 14,000 *g*. The supernatant was transferred to a 50-mL centrifuge tube. After adding 50 μL anti-MYC antibody (Chromo Tek, Catalog number ytmahydrochloric acid and 20% (v/v) methanol], and incubated in an oven at 65°C for 20 min. The seedlings were transferred to solution II [7% (w/v) sodium hydroxide and 60% (v/v) ethanol] and incubated at room temperature for 20 min. The seedlings were successively transferred to 60%, 40%, 20%, and 10% (v/v) anhydrous ethanol and incubated at room temperature for 10 min per step. The dehydrated seedlings were transferred to solution III [25% (v/v) glycerin and 5% (v/v) anhydrous ethanol] for long-term storage or placed on a slide to observe LR development and the proportions of LRP at each stage of development. To synchronize LR induction by gravitropic stimulation, 3-day-old *Pro35S:ERF13-MYC*, WT, and *mac3a mac3b* seedlings grown in the same Petri dish were simultaneously flipped 90 degrees for gravitropic stimulation. The LRP at the bends in roots of plants of different genotypes were counted at 18 h and 48 h. For more details, please see (Lucas et al., 2008; Peret et al., 2012).

Seedling treatment, RNA extraction, and RT-qPCR

To verify the effects of auxin on *MAC3A* and *MAC3B* transcript levels, 8-day-old WT seedlings

were treated with 10 μM NAA for 2, 4, 7, 10, 12, and 24 h, and ~0.1 g of root tissue was collected for total RNA extraction. To detect which core transcription factor was associated with the auxin-induced upregulation of *MAC3A* and *MAC3B*, 8-day-old WT, *arf7-1*, *arf19-1*, *arf7-1 arf19-1*, and *puchi-1* seedlings were treated with 10 μM NAA for 10 h or 12 h, and ~0.1 g of root tissue was collected for total RNA extraction. To determine whether auxin-induced *KCS16* transcription depends on MAC3A and MAC3B, 8-day-old WT and *mac3a mac3b* seedlings were treated with 10 μM NAA for 8 h, and ~0.1 g of root tissue was collected for total RNA extraction. Total RNA extraction and reverse transcription quantitative PCR (RT-qPCR) were performed as previously described (Yu et al., 2023). *ACTIN2* and *UBIQUITIN10* (*UBQ10*) were used as the reference genes. All primers used for these assays are listed in Supplemental Table S2.

rBiFC assay in Arabidopsis mesophyll protoplasts

Ratiometric BiFC (rBiFC) is an upgraded BiFC method that has been widely used to measure the strength of protein interactions (Hecker et al., 2015; Li et al., 2020; Tian et al., 2022). In brief, the CDS of $ERF13^{WT}$, $ERF13^{AAA}$, or $ERF13^{DDD}$ (Lv et al., 2021) and the CDS of $MAC3A^{\Delta U\text{-}box}$ (179−1,572 bp) or $MAC3B^{\Delta U\text{-}box}$ (179−1,578 bp) were simultaneously amplified and cloned into the same vector, *pBiFCt-2in1-NC* (Tian et al., 2022), which was used to transform Arabidopsis protoplasts, followed by incubation for 12 h. The protoplasts were prepared as previously described (Yu et al., 2023). Fluorescence was observed under a confocal microscope (Zeiss LSM 880, Germany). The propidium iodide signals were detected by using 488 nm laser excitation wavelength and 575 nm emission wavelength, and the GFP signals were detected by using 561 nm laser excitation wavelength and 500–530 nm emission wavelength. Primers used for the rBiFC assay are listed in Supplemental Table S2.

Co-IP assay in Arabidopsis mesophyll protoplasts

Co-IP was performed to investigate the effects of auxin on the strength of the ERF13–MAC3A and ERF13–MAC3B interactions. The CDS of *ERF13* was amplified and cloned into the *pSuper1300-MYC* vector (Feng et al., 2014) to generate ERF13-MYC; the CDS of *MAC3A* or *MAC3B* was amplified and cloned into the *pSuper1300-YFP* (Feng et al., 2014) vector to

construct MAC3A-YFP or MAC3B-YFP. The protoplasts were prepared as previously described (Yu et al., 2023). The protoplasts were divided into two groups: 10 μM NAA + 10 μM MG132 (26S proteasome inhibitor; APExBIO, Catalog number A2585, Houston, TX, USA) was added to one group, and 10 μM MG132 was added to the other group as a control. Both groups of protoplasts were incubated for 2 h. Anti-GFP antibody (Chromo Tek, Catalog number ytma, 1:100 dilution, Germany) was used to immunoprecipitate MAC3A-GFP or MAC3B-GFP, and anti-MYC antibody (ABclonal, Catalog number AE010, 1:5,000 dilution, Boston, MA, USA) was used to detect the level of ERF13-MYC.

For the Co-IP experiment to examine the interaction strength of MAC3A or MAC3B with ERF13^{WT}, ERF13^{AAA}, or ERF13^{DDD}, the CDS of *ERF13^{WT}*, *ERF13^{AAA}*, or *ERF13^{DDD}* was amplified and cloned into the *pSuper1300-MYC* vector to express ERF13^{WT}-MYC, ERF13^{AAA}-MYC, or ERF13^{DDD}-MYC; the CDS of *MAC3A* or *MAC3B* was amplified and cloned into the *pSuper1300-YFP* vector to express MAC3A-YFP or MAC3B-YFP. Combinations of the MYC and YFP constructs were used to transform protoplasts, followed by incubation for 12 h. Anti-GFP antibody (Chromo Tek, Catalog number ytma, 1:100 dilution, Germany) was used to immunoprecipitate MAC3A-YFP or MAC3B-YFP, and anti-MYC antibody (ABclonal, Catalog number AE010, 1:5,000 dilution, Boston, MA, USA) was used to detect the levels of ERF13^{WT}-MYC, ERF13^{AAA}-MYC, and ERF13^{DDD}-MYC. Primers used for the Co-IP assays are listed in Supplemental Table S2.

GUS staining

For GUS staining, 8-day-old *ProMAC3A:GUS*, *ProMAC3B:GUS*, and *ProERF13:GUS* seedlings were collected, infiltrated with GUS staining solution [2 mM 5-bromo-4-chloro-3-indolyl-b-D-glucuronide (X-Gluc; Goldbio, St. Louis, MO, USA), 2 mM $K_3[Fe(CN)_6]$, 100 mM sodium phosphate buffer (pH 7.2), 2 mM $K_4Fe(CN)_6$, 0.1% Triton X-100, and 10 mM Na_2EDTA], and incubated in a 37°C oven for 3 h. The seedlings were transferred to decolorizing solution [acetic acid:ethanol (v/v) = 3:1] and treated for approximately 8 h until the leaves were transparent. The seedlings were successively transferred to 70%, 50%, 30%, and 10% (v/v) ethanol and incubated at room temperature for 10 min per step for decolorization and visualization. The decolorized seedlings were observed under a microscope (Olympus

BX53, Tokyo, Japan).

LCI assay

LCI assays were performed as previously described (Yu et al., 2023). In brief, the CDS of *MAC3A*, *MAC3B*, *MAC3A*$^{\Delta U\text{-}box}$, or *MAC3B*$^{\Delta U\text{-}box}$ was cloned in-frame with the CDS of *nLUC* in the *JW771* vector (Cui et al., 2023) to generate MAC3A-nLUC, MAC3B-nLUC, MAC3A$^{\Delta U\text{-}box}$-nLUC, or MAC3B$^{\Delta U\text{-}box}$-nLUC, and the CDS of *ERF13* was cloned in-frame with the CDS of *cLUC* in the *JW772* vector (Cui et al., 2023) to generate cLUC-ERF13. The constructed vectors and empty vectors were individually transformed into *Agrobacterium tumefaciens* strain GV3101 and infiltrated into different regions of 30-day-old *Nicotiana benthamiana* leaves in the following pairs: cLUC-ERF13 or cLUC + MAC3A-nLUC, MAC3B-nLUC, MAC3A$^{\Delta U\text{-}box}$-nLUC, MAC3B$^{\Delta U\text{-}box}$-nLUC, or nLUC. Following incubation in the dark at 26°C for 12 h, the infiltrated *Nicotiana benthamiana* were incubated under a normal photoperiod (16-h light/8-h dark) at 26°C for 60 h. The leaves were treated with D-luciferin potassium salt (Meilunbio, Dalian, China) for 5–10 min and visualized with a Tanon-5200 Multi imaging system (Tanon, Shanghai, China). To verify the interaction of full-length MAC3A and MAC3B with ERF13, the *N. benthamiana* leaves were sprayed with 200 μM MG132 for 6 h prior to luminescence observation. Primers used in the LCI assays are listed in Supplemental Table S2.

Cell-free assay and calculation of protein half-life

Cell-free assays were performed as previously described (Yu et al., 2023). In brief, total proteins were extracted from 12-day-old *Pro35S:MAC3B-MYC*, WT, and *mac3a mac3b* seedlings with pre-cooled nondenaturing protein extraction buffer [5 mM DTT, 10 mM NaCl, 25 mM Tris-HCl (pH 7.5), 10 mM $MgCl_2$, 10 mM adenosine 5′-triphosphate, and 4 mM phenylmethylsulfonyl fluoride]. Purified recombinant GST-ERF13 protein was added to different protein extracts, followed by incubation at 4°C for 15, 30, 45, or 60 min. To detect the abundance of GST-ERF13 in protein extracts from *Pro35S:MAC3B-MYC*, WT, and *mac3a mac3b* plants, immunoblotting with anti-GST antibody (TransGen, Catatlog number HT601, Beijing, China) was performed at the indicated time points. After quantifying the protein signal

intensity with ImageJ (version 1.46r), the linear regression equation and half-life of GST-ERF13 in different protein extracts were calculated as described previously (Yu et al., 2019).

Ubiquitination assays in Arabidopsis mesophyll protoplasts

The CDS of *UBQ10* was amplified and cloned into *pCAMBIA1300-MYC* (Tang et al., 2012) to generate Ubiquitin-MYC; the CDS of *MAC3A* or *MAC3B* was amplified and cloned into *pSuper1300-GFP* to generate MAC3A-GFP or MAC3B-GFP; and the CDS of *ERF13* was amplified and cloned into *pSuper1300-FLAG* to generate ERF13-FLAG. Different combinations of these constructs were used to transform protoplasts, followed by incubation for 12 h. Protoplast preparation and transformation were performed as previously described (Yu et al., 2023). Before protein immunoprecipitation, 500 μL of protoplasts were transferred to 2-mL centrifuge tubes, incubated at room temperature for 20 min, and centrifuged at 200 *g* for 2 min. After removing the supernatant, SDS loading buffer was added to terminate the reaction, and the sample was stored at −80°C as an input sample. A 5-mL aliquot of protoplasts was transferred to a 10-mL centrifuge tube, and 200 μL lysis buffer was added immediately to the sample, followed by incubation at 4°C for 30 min, during which the protoplasts were gently shaken every 10 min. The sample was centrifuged at 4°C at 20,000 *g* for 10 min, and the supernatant was transferred to a pre-cooled 2-mL centrifuge tube. A 7-μL aliquot of anti-FLAG antibody-coupled beads (Bio-Link, Catalog number CH220110, 1:100 dilution, Shanghai, China) was placed in a new 2-mL centrifuge tube. The beads were washed three times in dilution buffer, added to the sample, and incubated at 4°C for 2 h. The beads were washed three times in dilution buffer with 1% (v/v) Triton X-100 and once in 50 mM Tris-HCl (pH 7.5). Finally, the reaction was terminated by adding SDS loading buffer, and anti-MYC antibody (ABclonal, Catalog number AE010, 1:5,000 dilution, Boston, MA, USA) was used to detect the ubiquitination levels of ERF13-FLAG (or the coupling intensity of ERF13-FLAG and Ubiquitin-MYC) in the presence of MAC3A-GFP, MAC3B-GFP, or GFP.

Yeast one-hybrid assay

Yeast one-hybrid assay was performed as previously described (Lv et al., 2021) with the Matchmaker One-Hybrid Library Construction and Screening Kit (Clontech, Dongjing, Japan).

In brief, the CDS of *ARF7* or *ARF19* was amplified and cloned into the *pGADT7* (AD, Clontech, Cat#630442, Dongjing, Japan) vector, and the target DNA sequences of the *MAC3A-1* (-1,611 bp−-2,731 bp) and *MAC3A-2* (-133 bp−-1,157 bp) fragments of the *MAC3A* promoter and *MAC3B-1* (-1648 bp−-2813 bp) and *MAC3B-2* (-558 bp−-1,669 bp) fragments of the *MAC3B* promoter were amplified and cloned into the *pHIS2.1* vector. Each of the constructs was transferred separately into Y187 yeast using the Polyethylene glycol/Lithium Acetate (PEG/LiAc) method. After culturing on synthetic medium plates (SD medium) lacking Trp and Leu (−WL) for two days, the transformants were transferred onto SD medium lacking Trp, Leu, and Ade (SD−WLA) for 2−3 days before observation. Primers used in the Y1H assay are listed in Supplemental Table S2.

Statistical analysis

Statistical analysis was performed using Student's *t*-test (ns, no significant difference; *, $P<0.05$; **, $P<0.01$; ***, $P<0.001$) or One-way ANOVA ($P<0.05$; LSD and Duncan test) with SPSS software (version 25). All experiments had at least three biological replicates, and the data are presented as mean ± standard error (SE). Details of all the statistical analyses performed in this study are shown in Supplemental Data Set S1.

Accession numbers

Sequence data from this article can be found in the GenBank/EMBL libraries under the following accession numbers: *MAC3A* (AT1G04510), *MAC3B* (AT2G33340), *MPK14* (AT4G36450), *ERF13* (AT2G44840), *ARF7* (AT5G20730), *ARF19* (AT1G19220), *EXP14* (AT5G56320), *EXP17* (AT4G01630), *KCS8* (AT2G15090), *KCS16* (AT4G34250), *KCS18* (AT4G34520), *LBD16* (AT2G42430), *LBD18* (AT2G45420), *LBD29* (AT3G58190), and *PUCHI* (AT5G18560).

Supplemental data

Supplemental Figure S1. LCI assays in *N. benthamiana* leaves treated with MG132.

Supplemental Figure S2. Expression pattern of *MAC3A* in primary root tip.

Supplemental Figure S3. Characterization of the *mac3a* and *mac3b* mutants.

Supplemental Figure S4. Root lengths of WT, *mac3a-1*, *mac3a-2*, *mac3b-2*, *mac3a mac3b*, and *ProMAC3A:MAC3A-GFP/mac3a mac3b*.

Supplemental Figure S5. Phenotypes of *mac3a mac3b* LRs in response to auxin.

Supplemental Figure S6. Percentages of LRs at different developmental stages in different plant materials.

Supplemental Figure S7. Percentage of LRs in 3-day-old WT, *Pro35S:ERF13-MYC#6*, and *mac3a mac3b* at different stages of LRP development after 18 h of gravity treatment.

Supplemental Figure S8. Transcript levels of LR-related genes in *Pro35S:GFP-ERF13* and *mac3a mac3b*.

Supplemental Figure S9. Phenotypes of the LRs of *MAC3A*-and *MAC3B*-overexpressing lines.

Supplemental Figure S10. *KCS8* and *KCS16* transcript levels in *Pro35S:GFP-ERF13/ Pro35S:MAC3B-MYC* lines.

Supplemental Figure S11. Expression patterns of *ERF13* in LRP.

Supplemental Figure S12. MAC3B degrades ERF13 in roots.

Supplemental Figure S13. *KCS16* transcript levels in WT and *mac3a mac3b* treated with or without NAA.

Supplemental Figure S14. Validation of the binding of ARF7 and ARF19 to the *MAC3A* and *MAC3B* promoters.

Supplemental Figure S15. Protein stability of MAC3A and MAC3B in response to NAA.

Supplemental Table S1. Candidate ERF13-interacting proteins identified by IP-MS.

Supplemental Table S2. Primers used in this study.

Supplemental Data Set S1. Results of statistical analysis.

Funding information

This work was supported by grants from the National Natural Science Foundation of China [32170338 (Z.D.), 32061143005 (Z.D.), 32000225 (Z.Y.), and 32170313 (B.L.)] and by the Taishan Scholar Special Project Fund of Shandong Province (Z.D).

Acknowledgments

We thank Prof. Shengjun Li (Qingdao Institute of Bioenergy and Bioprocess Technology,

Chinese Academy of Sciences) for sharing published materials. We also thank Jie Dai at Shanghai Bioprofile Technology Co. Ltd. for his technical support in mass spectroscopy.

Author Contributions

Designed research: Z.Y. and Z.D.; Performed research: X.Q., Z.Y., B.L., X.L., J.S., and Q.Y.; Analyzed data: X.Q. and Z.Y.; Supervision: Z.Y. and Z.D.; Wrote the paper: Z.Y. and Z.D.

Declaration of interests

The authors declare that they have no competing interests.

Data and materials availability

All data needed to evaluate the conclusions in the paper are present in the paper and/or Supplemental Materials.

References

Banda, J., Bellande, K., von Wangenheim, D., Goh, T., Guyomarc'h, S., Laplaze, L., and Bennett, M.J. (2019). Lateral Root Formation in Arabidopsis: A Well-Ordered LRexit. Trends Plant Sci **24,** 826-839.

Cui, M.H., Li, Y.P., Li, J.H., Yin, F.X., Chen, X.Y., Qin, L.M., Wei, L., Xia, G.M., and Liu, S.W. (2023). Ca2+-dependent TaCCD1 cooperates with TaSAUR215 to enhance plasma membrane H plus -ATPase activity and alkali stress tolerance by inhibiting PP2C-mediated dephosphorylation of TaHA2 in wheat. Molecular Plant **16,** 571-587.

Fan, M.Z., Xu, C.Y., Xu, K., and Hu, Y.X. (2012). LATERAL ORGAN BOUNDARIES DOMAIN transcription factors direct callus formation in regeneration. Cell Res **22,** 1169-1180.

Feke, A., Liu, W., Hong, J., Li, M.W., Lee, C.M., Zhou, E.K., and Gendron, J.M. (2019). Decoys provide a scalable platform for the identification of plant E3 ubiquitin ligases that regulate circadian function. Elife **8**.

Feke, A.M., Hong, J., Liu, W., and Gendron, J.M. (2020). A Decoy Library Uncovers U-Box E3 Ubiquitin Ligases That Regulate Flowering Time in Arabidopsis. Genetics **215,** 699-712.

Feng, C.Z., Chen, Y., Wang, C., Kong, Y.H., Wu, W.H., and Chen, Y.F. (2014). Arabidopsis RAV1 transcription factor, phosphorylated by SnRK2 kinases, regulates the expression of ABI3, ABI4, and ABI5 during seed germination and early seedling development. Plant Journal **80,** 654-668.

Goh, T., Joi, S., Mimura, T., and Fukaki, H. (2012). The establishment of asymmetry in lateral root founder cells is regulated by LBD16/ASL18 and related LBD/ASL proteins. Development **139,** 883-893.

Goh, T., Toyokura, K., Yamaguchi, N., Okamoto, Y., Uehara, T., Kaneko, S., Takebayashi, Y., Kasahara, H., Ikeyama, Y., Okushima, Y., Nakajima, K., Mimura, T., Tasaka, M., and Fukaki, H. (2019). Lateral root initiation requires the sequential induction of transcription factors LBD16 and PUCHI in. New Phytologist **224,** 749-760.

Hecker, A., Wallmeroth, N., Peter, S., Blatt, M.R., Harter, K., and Grefen, C. (2015). Binary 2in1 Vectors Improve

in Planta (Co)localization and Dynamic Protein Interaction Studies. Plant Physiol **168,** 776-787.

Huang, R., Zheng, R., He, J., Zhou, Z., Wang, J., Xiong, Y., and Xu, T. (2019). Noncanonical auxin signaling regulates cell division pattern during lateral root development. Proc Natl Acad Sci U S A **116,** 21285-21290.

Jia, T., Zhang, B., You, C., Zhang, Y., Zeng, L., Li, S., Johnson, K.C.M., Yu, B., Li, X., and Chen, X. (2017). The Arabidopsis MOS4-Associated Complex Promotes MicroRNA Biogenesis and Precursor Messenger RNA Splicing. Plant Cell **29,** 2626-2643.

Karlova, R., Boer, D., Hayes, S., and Testerink, C. (2021). Root plasticity under abiotic stress. Plant Physiol **187,** 1057-1070.

Li, J.G., Fan, M., Hua, W., Tian, Y., Chen, L.G., Sun, Y., and Bai, M.Y. (2020). Brassinosteroid and Hydrogen Peroxide Interdependently Induce Stomatal Opening by Promoting Guard Cell Starch Degradation. Plant Cell **32,** 984-999.

Li, S., Liu, K., Zhou, B., Li, M., Zhang, S., Zeng, L., Zhang, C., and Yu, B. (2018). MAC3A and MAC3B, Two Core Subunits of the MOS4-Associated Complex, Positively Influence miRNA Biogenesis. Plant Cell **30,** 481-494.

Li, Y., Yang, J., Shang, X., Lv, W., Xia, C., Wang, C., Feng, J., Cao, Y., He, H., Li, L., and Ma, L. (2019). SKIP regulates environmental fitness and floral transition by forming two distinct complexes in Arabidopsis. New Phytol **224,** 321-335.

Liu, H.L., Wang, G.C., Feng, Z.H., and Zhu, J.A. (2010). Screening of genes associated with dedifferentiation and effect of LBD29 on pericycle cells in Arabidopsis thaliana. Plant Growth Regul **62,** 127-136.

Lucas, M., Godin, C., Jay-Allemand, C., and Laplaze, L. (2008). Auxin fluxes in the root apex co-regulate gravitropism and lateral root initiation. J Exp Bot **59,** 55-66.

Lv, B., Wei, K., Hu, K., Tian, T., Zhang, F., Yu, Z., Zhang, D., Su, Y., Sang, Y., Zhang, X., and Ding, Z. (2021). MPK14-mediated auxin signaling controls lateral root development via ERF13-regulated very-long-chain fatty acid biosynthesis. Mol Plant **14,** 285-297.

Malamy, J.E., and Benfey, P.N. (1997). Organization and cell differentiation in lateral roots of Arabidopsis thaliana. Development **124,** 33-44.

Monaghan, J., Xu, F., Gao, M., Zhao, Q., Palma, K., Long, C., Chen, S., Zhang, Y., and Li, X. (2009). Two Prp19-like U-box proteins in the MOS4-associated complex play redundant roles in plant innate immunity. PLoS Pathog **5,** e1000526.

Ninoles, R., Planes, D., Arjona, P., Ruiz-Pastor, C., Chazarra, R., Renard, J., Bueso, E., Forment, J., Serrano, R., Kranner, I., Roach, T., and Gadea, J. (2022). Comparative analysis of wild-type accessions reveals novel determinants of Arabidopsis seed longevity. Plant Cell Environ **45,** 2708-2728.

Okushima, Y., Fukaki, H., Onoda, M., Theologis, A., and Tasaka, M. (2007). ARF7 and ARF19 regulate lateral root formation via direct activation of genes in. Plant Cell **19,** 118-130.

Okushima, Y., Overvoorde, P.J., Arima, K., Alonso, J.M., Chan, A., Chang, C., Ecker, J.R., Hughes, B., Lui, A., Nguyen, D., Onodera, C., Quach, H., Smith, A., Yu, G., and Theologis, A. (2005). Functional genomic analysis of the AUXIN RESPONSE FACTOR gene family members in Arabidopsis thaliana: unique and overlapping functions of ARF7 and ARF19. Plant Cell **17,** 444-463.

Peret, B., Li, G., Zhao, J., Band, L.R., Voss, U., Postaire, O., Luu, D.T., Da Ines, O., Casimiro, I., Lucas, M., Wells, D.M., Lazzerini, L., Nacry, P., King, J.R., Jensen, O.E., Schaffner, A.R., Maurel, C., and Bennett, M.J. (2012). Auxin regulates aquaporin function to facilitate lateral root emergence. Nat Cell Biol **14,** 991-998.

Shang, E.L., Wang, X., Li, T.H., Guo, F.F., Ito, T., and Sun, B. (2021). Robust control of floral meristem determinacy

by position-specific multifunctions of KNUCKLES. P Natl Acad Sci USA **118**.

Tang, G.L., Yan, J., Gu, Y.Y., Qiao, M.M., Fan, R.W., Mao, Y.P., and Tang, X.Q. (2012). Construction of short tandem target mimic (STTM) to block the functions of plant and animal microRNAs. Methods **58,** 118-125.

Tian, Y., Zhao, N., Wang, M., Zhou, W., Guo, J., Han, C., Zhou, C., Wang, W., Wu, S., Tang, W., Fan, M., and Bai, M.Y. (2022). Integrated regulation of periclinal cell division by transcriptional module of BZR1-SHR in Arabidopsis roots. New Phytol **233,** 795-808.

Trinh, D.C., Lavenus, J., Goh, T., Boutté, Y., Drogue, Q., Vaissayre, V., Tellier, F., Lucas, M., Voss, U., Gantet, P., Faure, J.D., Dussert, S., Fukaki, H., Bennet, M.J., Laplaze, L., and Guyomarc'h, S. (2019). PUCHI regulates very long chain fatty acid biosynthesis during lateral root and callus formation. P Natl Acad Sci USA **116,** 14325-14330.

Tu, Y.T., Chen, C.Y., Huang, Y.S., Chang, C.H., Yen, M.R., Hsieh, J.A., Chen, P.Y., and Wu, K. (2022). HISTONE DEACETYLASE 15 and MOS4-associated complex subunits 3A/3B coregulate intron retention of ABA-responsive genes. Plant Physiol **190,** 882-897.

Wiborg, J., O'Shea, C., and Skriver, K. (2008). Biochemical function of typical and variant Arabidopsis thaliana U-box E3 ubiquitin-protein ligases. Biochem J **413,** 447-457.

Yu, Z., Zhang, F., Friml, J., and Ding, Z. (2022). Auxin signaling: Research advances over the past 30 years. J Integr Plant Biol **64,** 371-392.

Yu, Z., Ma, J., Zhang, M., Li, X., Sun, Y., Zhang, M., and Ding, Z. (2023). Auxin promotes hypocotyl elongation by enhancing BZR1 nuclear accumulation in Arabidopsis. Sci Adv **9**, eade2493.

Yu, Z., Zhang, D., Xu, Y., Jin, S., Zhang, L., Zhang, S., Yang, G., Huang, J., Yan, K., Wu, C., and Zheng, C. (2019). CEPR2 phosphorylates and accelerates the degradation of PYR/PYLs in Arabidopsis. J Exp Bot **70,** 5457-5469.

Zhang, F., Tao, W.Q., Sun, R.Q., Wang, J.X., Li, C.L., Kong, X.P., Tian, H.Y., and Ding, Z.J. (2020). PRH1 mediates ARF7-LBD dependent auxin signaling to regulate lateral root development in. Plos Genetics **16**.

Zhu, Q., Shao, Y., Ge, S., Zhang, M., Zhang, T., Hu, X., Liu, Y., Walker, J., Zhang, S., and Xu, J. (2019). A MAPK cascade downstream of IDA-HAE/HSL2 ligand-receptor pair in lateral root emergence. Nat Plants **5,** 414-423.

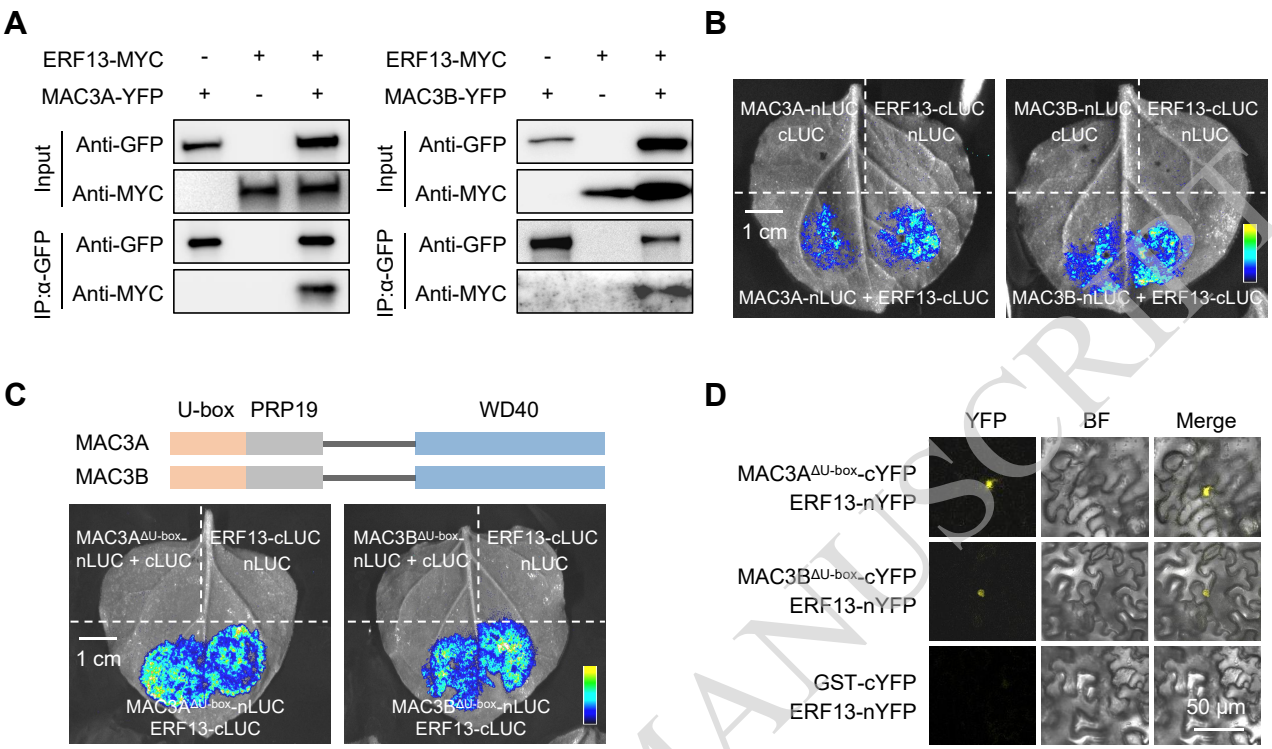

Figure 1. ERF13 interacts with MAC3A and MAC3B.
(A) Co-IP experiments in Arabidopsis protoplasts verifying the interactions between ERF13 and the E3 ligases MAC3A and MAC3B. Immunoprecipitation was performed with anti-GFP antibody, and interactions with ERF13-MYC were detected with anti-MYC antibody. Co-IP: co-immunoprecipitation. GFP: green fluorescent protein. YFP: yellow fluorescent protein. **(B and C)** LCI assays in *N. benthamiana* leaves validating the interactions of ERF13–MAC3A and ERF13–MAC3B (B) and ERF13–MAC3A$^{\Delta U\text{-box}}$ and ERF13–MAC3B$^{\Delta U\text{-box}}$ (C). The color scale from dark blue to yellow reflects the intensity of protein interaction from weak to strong. LCI: luciferase complementation imaging. nLUC: the n-terminus of luciferase. cLUC: the c-terminus of luciferase. Bar, 1 cm. (D) BiFC assays in *N. benthamiana* leaves verifying the interactions of ERF13 with MAC3A$^{\Delta U\text{-box}}$ and MAC3B$^{\Delta U\text{-box}}$. BiFC: bimolecular fluorescence complementation. BF: bright field. Bar, 50 μm. Similar results were obtained from three independent experiments; panel A displays a representative image obtained from one gel-based assay.

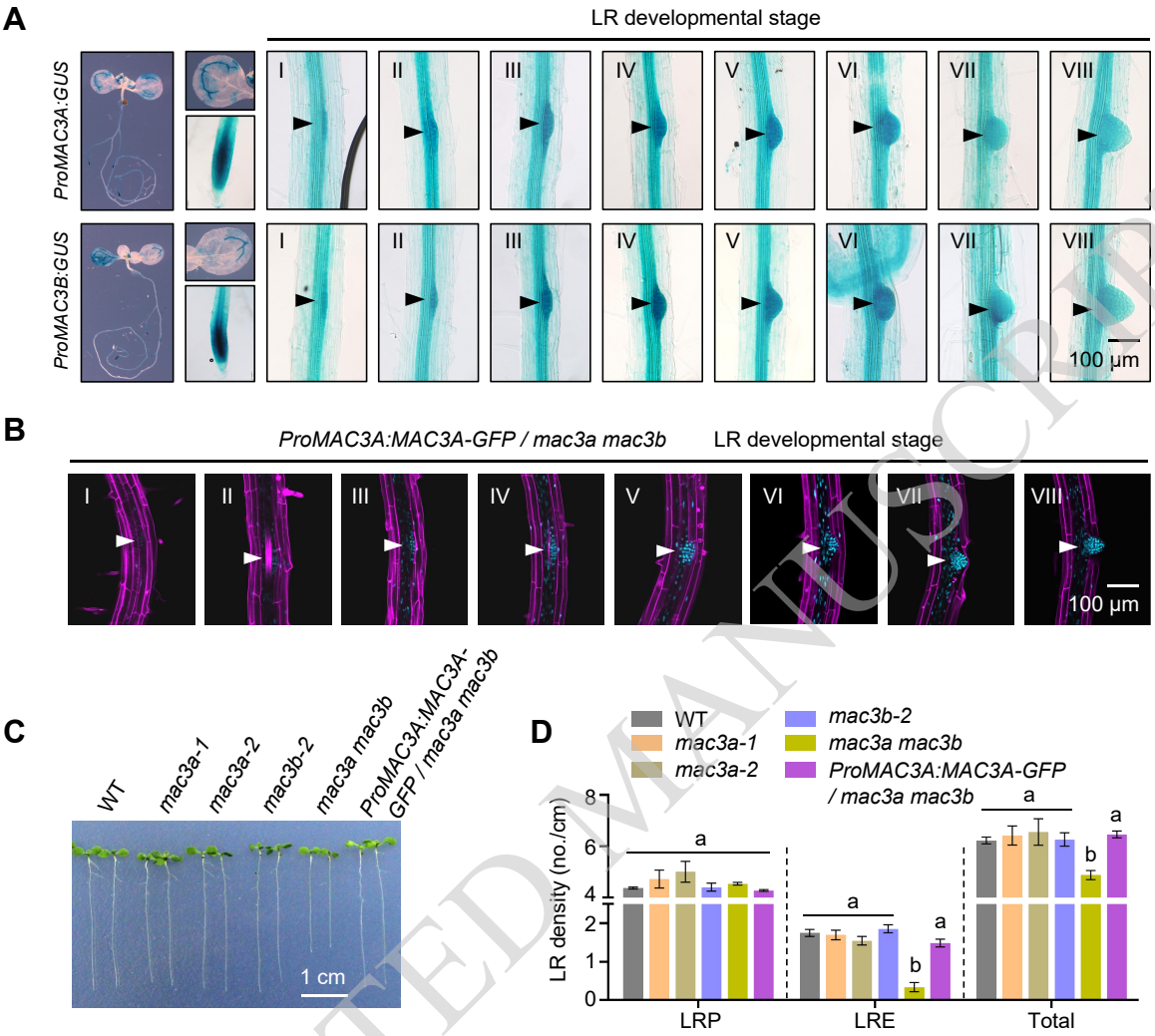

Figure 2. MAC3A and MAC3B regulate LR development.
(A) GUS staining images of 8-day-old *ProMAC3A:GUS* and *ProMAC3B:GUS* seedlings. Arrowheads indicate the eight stages of LRP development. Bar, 100 μm. GUS: histochemical β-glucuronidase. WT: wild type. LR: lateral root. LRP: lateral root primordium. **(B)** Fluorescence images of the LRP of 8-day-old *ProMAC3A:MAC3A-GFP/mac3a mac3b* seedlings. In all fluorescent images, we replaced green (MAC3A-GFP signal) with bright blue and red (propidium iodide signal) with magenta. Bar, 100 μm. **(C)** Phenotypes of the LRs of WT, *mac3a-1*, *mac3a-2*, *mac3b-2*, *mac3a mac3b*, and *ProMAC3A:MAC3A-GFP/mac3a mac3b* seedlings grown in 1/2 MS medium for 8 days. Bar, 1 cm. **(D)** LR density of the seedlings shown in (C). Three independent biological replicates produced similar results, and at least 80 seedlings per line were used for statistical analysis. LRE: lateral root emergence. Total = LRP + LRE. One-way ANOVA; $P<0.01$.

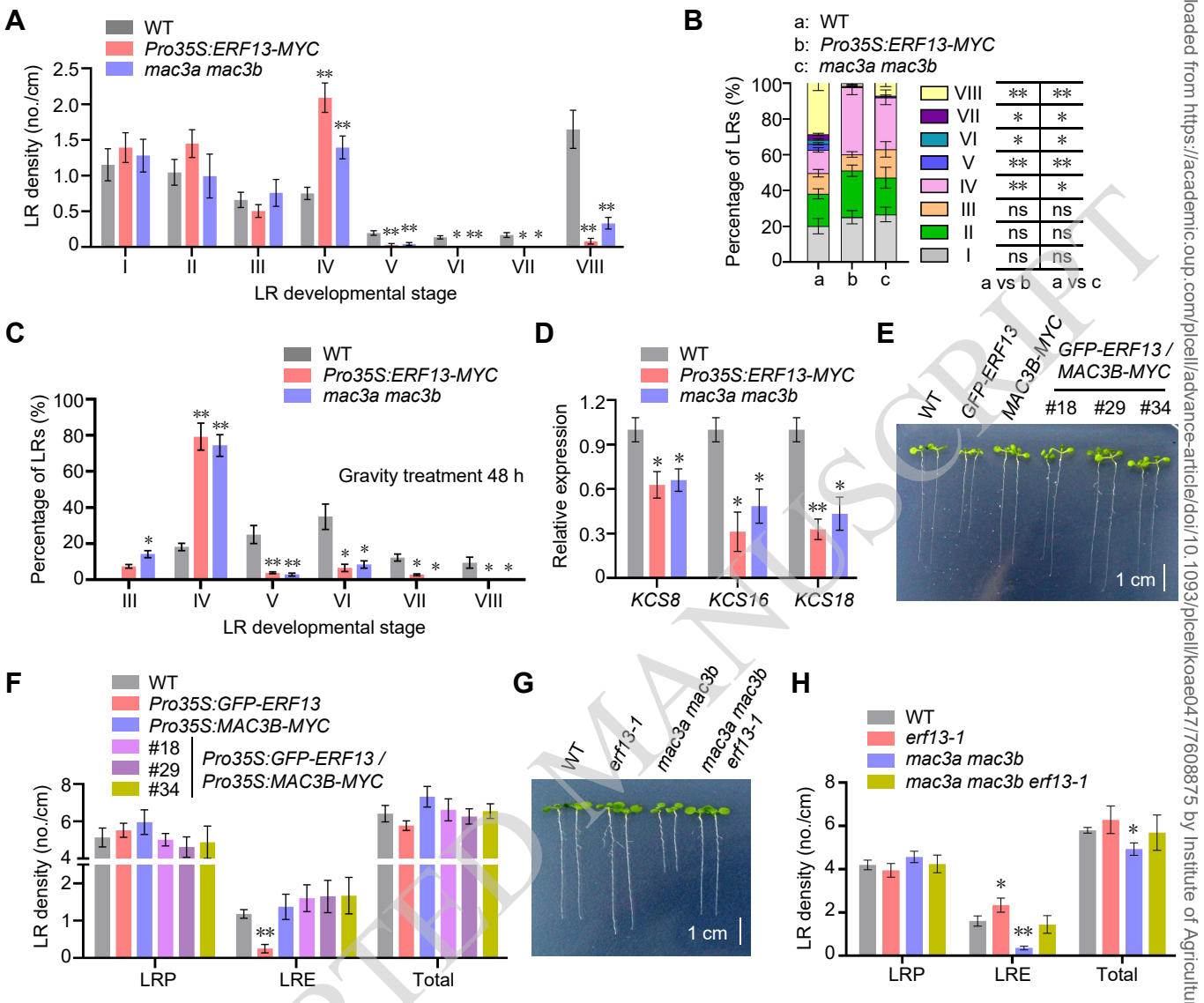

Figure 3. ERF13 and the E3 ligases MAC3A and MAC3B antagonistically regulate LRP development.
(A) Densities of LRs at different stages of development in 8-day-old WT, *Pro35S:ERF13-MYC#6*, and *mac3a mac3b* seedlings. Three independent biological replicates produced similar results, and at least 55 seedlings per line were used for statistical analysis. *Pro35S:ERF13-MYC*#6 and *mac3a mac3b* were separately compared with the WT. Student's t-test; *, $P<0.05$; **, $P<0.01$. WT: wild type. **(B)** Percentages of LRs at different stages of development in 8-day-old WT, *Pro35S:ERF13-MYC*#6, and *mac3a mac3b* seedlings. Student's *t*-test; ns, no significant difference; *, $P<0.05$; **, $P<0.01$. **(C)** Percentages of LRs at different stages of development in 3-day-old WT, *Pro35S:ERF13-MYC*#6, and *mac3a mac3b* seedlings after a 48-h gravity treatment. Three independent biological replicates produced similar results, and at least 40 seedlings per line were used for statistical analysis. *Pro35S:ERF13-MYC*#6 and *mac3a mac3b* were compared with the WT. Student's *t*-test; *, $P<0.05$; **, $P<0.01$. **(D)** *KCS8*, *KCS16*, and *KCS18* transcript levels in the roots of 8-day-old WT, *Pro35S:ERF13-MYC*#6, and *mac3a mac3b* seedlings. *Pro35S:ERF13-MYC*#6 and *mac3a mac3b* were compared with the WT. Student's t-test; *, $P<0.05$; **, $P<0.01$. **(E)** Phenotypes of the LRs of WT, *Pro35S:GFP-ERF13*, *Pro35S:MAC3B-MYC*, and *Pro35S:GFP-ERF13/Pro35S:MAC3B-MYC* seedlings grown in 1/2 MS medium for 8 days. Bar, 1 cm. **(F)** LR densities of the seedlings shown in (E). Three independent biological replicates produced similar results, and at least 45 seedlings per line were used for statistical analysis. All plant materials were compared with the WT. Student's t-test; **, $P<0.01$. **(G)** Phenotypes of the LRs of 8-day-old WT, *erf13-1*, *mac3a mac3b*, and *mac3a mac3b erf13-1* seedlings. Bar, 1 cm. (H) LR densities of the seedlings shown in (G). Three independent biological replicates produced similar results, and at least 30 seedlings per line were used for statistical analysis. All plant materials were compared with the WT. Student's t-test; *, $P<0.05$; **, $P<0.01$.

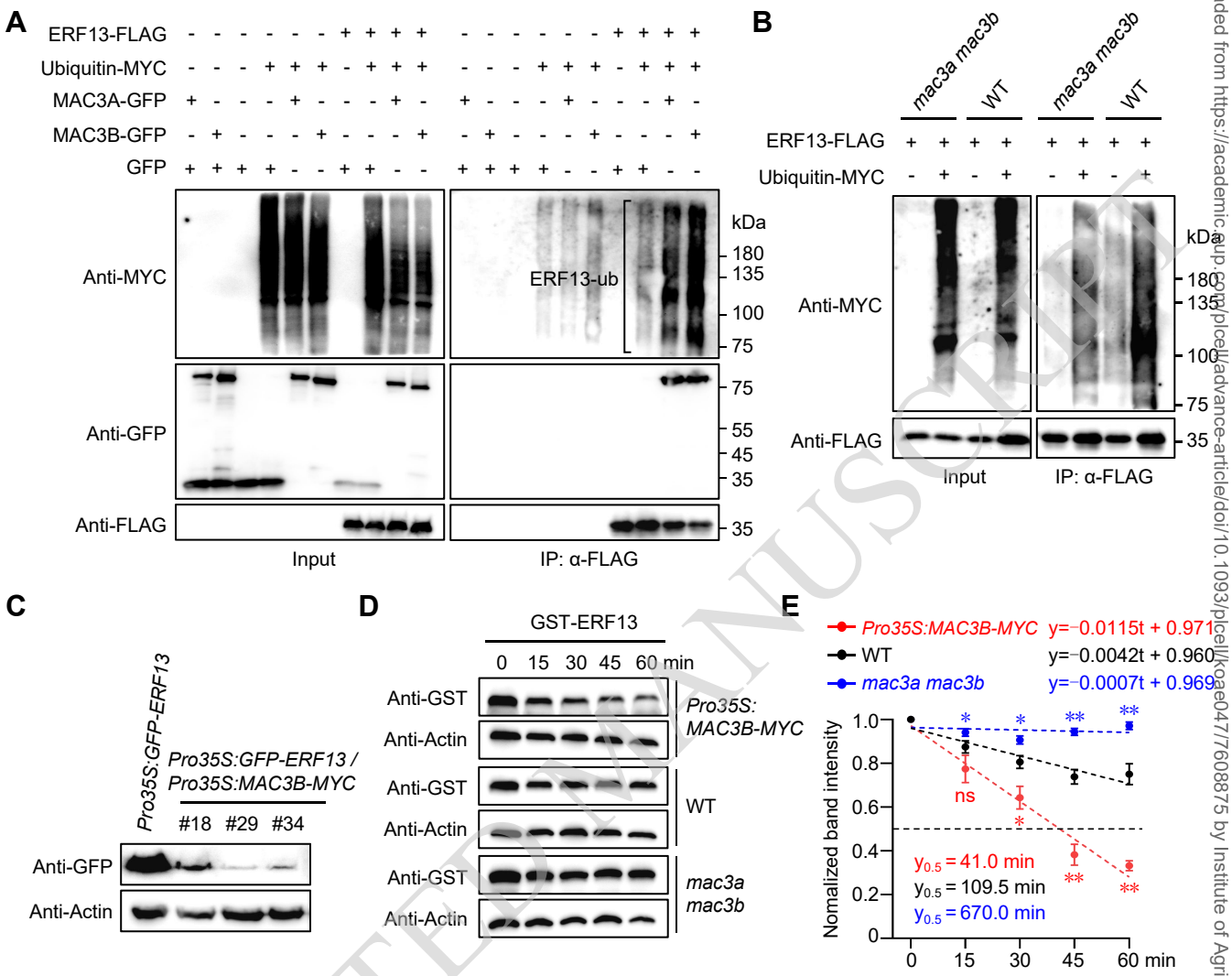

Figure 4. MAC3A and MAC3B ubiquitinate and degrade ERF13.

(A) Ubiquitination of ERF13-FLAG in the presence or absence of the E3 ligases MAC3A and MAC3B detected in an Arabidopsis protoplast transient transformation assay. Anti-FLAG antibody was used to immunoprecipitate ERF13-FLAG, and anti-MYC antibody was used to detect Ubiquitin-MYC. GFP: green fluorescent protein. **(B)** Ubiquitination of ERF13-FLAG in WT and *mac3a mac3b* detected in an Arabidopsis protoplast transient transformation assay. Anti-FLAG antibody was used to immunoprecipitate ERF13-FLAG, and anti-MYC antibody was used to detect Ubiquitin-MYC. WT: wild type. IP: immunoprecipitation. **(C)** Immunoblot analysis of *Pro35S:GFP-ERF13* and different *Pro35S:GFP-ERF13/Pro35S:MAC3B-MYC* lines probed with the indicated antibodies. **(D)** Degradation rates of GST-ERF13 in cell-free assays using *Pro35S:MAC3B-MYC*, WT, and *mac3a mac3b* protein extracts. Recombinant purified ERF13-GST was added to the protein extracts and incubated for 15, 30, 45, or 60 min. Protein abundance was determined with anti-GST antibody. **(E)** Linear regressions of the quantified band intensities from (D) by ImageJ representing the degradation rates of GST-ERF13 in *Pro35S:MAC3B-MYC*, WT, and *mac3a mac3b* protein extracts. y0.5 represents the time point at which half of the protein was degraded. Similar results were obtained from three independent experiments. Each figure panel displays a representative image obtained from a gel-based assay. All plant materials were compared with WT separately. Student's t-test; ns: no significant difference; *, $P<0.05$; **, $P<0.01$.

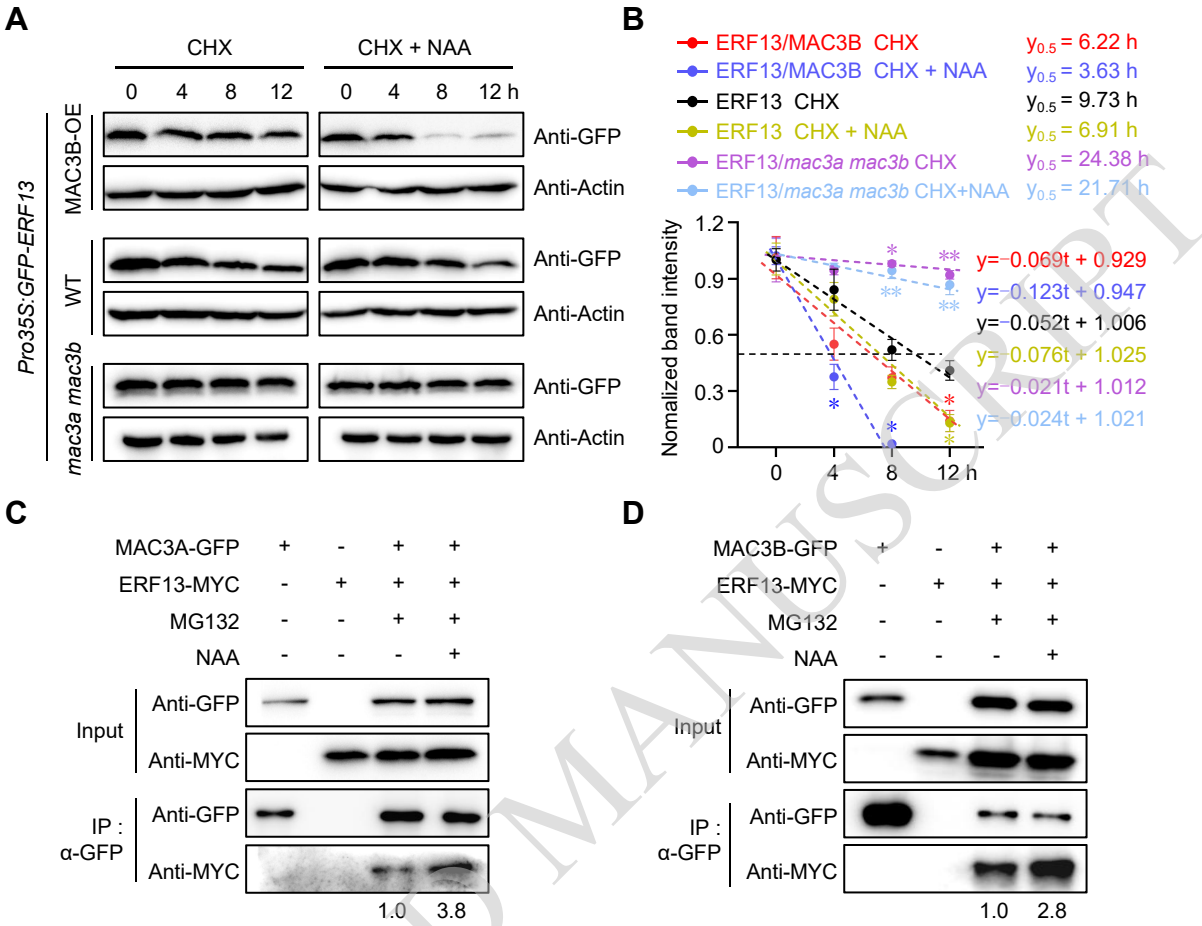

Figure 5. MAC3A and MAC3B regulate auxin-induced degradation of ERF13.
(A) Degradation rates of ERF13 in *Pro35S:GFP-ERF13*, *Pro35S:GFP-ERF13/Pro35S:MAC3B-MYC*, and *Pro35S:GFP-ERF13/mac3a mac3b* seedlings treated with or without NAA. Seedlings were treated with 200 μM CHX or 200 μM CHX + 10 μM NAA for 4, 8, or 12 h. CHX: cycloheximide. WT: wild type. MAC3B-OE: *Pro35S:MAC3B-MYC*. NAA: naphthaleneacetic acid. Similar results were obtained from three independent experiments. Each figure panel displays a representative image obtained from a gel-based assay. **(B)** Linear regressions of the quantified band intensities from (A) by ImageJ representing the degradation rates of GFP-ERF13 in *Pro35S:GFP-ERF13*, *Pro35S:GFP-ERF13/Pro35S:MAC3B-MYC*, and *Pro35S:GFP-ERF13/mac3a mac3b* with or without NAA treatment. y0.5 represents the time point at which half of the ERF13-GFP protein was degraded. All groups were compared with *Pro35S:GFP-ERF13*-CHX separately. Student's t-test; *, $P<0.05$; **, $P<0.01$. **(C and D)** Co-IP experiments in Arabidopsis protoplasts examining the effects of NAA on the interaction between ERF13 and MAC3A (C) and ERF13 and MAC3B (D). Anti-GFP antibody was used to immunoprecipitate MAC3A-GFP or MAC3B-GFP, and anti-MYC antibody was used to detect ERF13-MYC levels. Similar results were obtained from three independent experiments, whose averages are indicated below the figure. Each figure panel displays a representative image obtained from a gel-based assay. IP: immunoprecipitation.

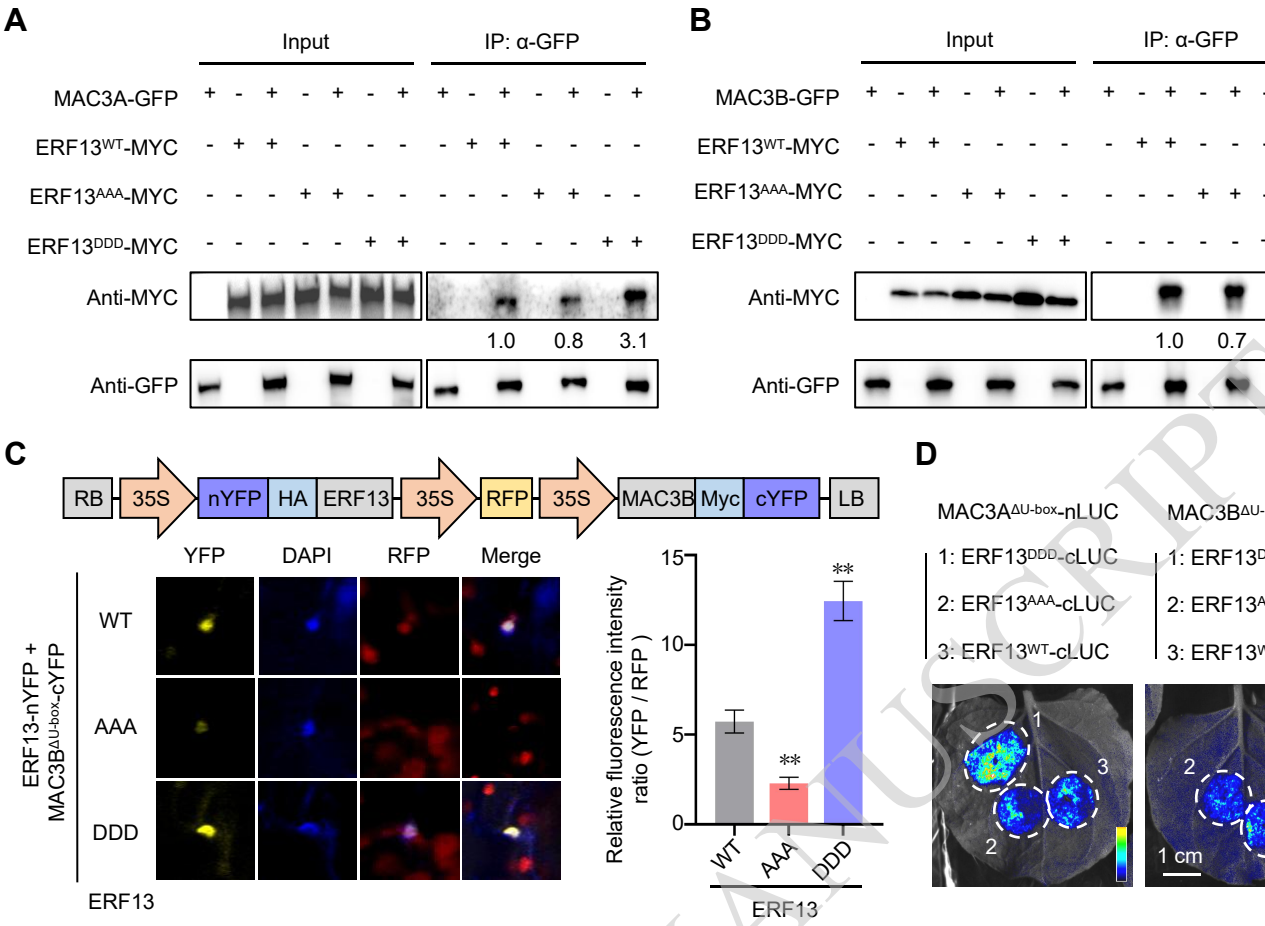

Figure 6. MAC3A and MAC3B preferentially interact with and degrade MPK14-phosphorylated ERF13.
(A and B) Co-IP experiments in Arabidopsis protoplasts examining the interaction strength of MAC3A (A) or MAC3B (B) with ERF13^{WT}, ERF13^{AAA}, and ERF13^{DDD}. Anti-GFP antibody was used to immunoprecipitate MAC3A-GFP or MAC3B-GFP, and anti-MYC antibody was used to detect the protein levels of ERF13^{WT}-MYC, ERF13^{AAA}-MYC, and ERF13^{DDD}-MYC. Co-IP: co-immunoprecipitation. GFP: green fluorescent protein. IP: immunoprecipitation. **(C)** A quantitative BiFC experiment in *N. benthamiana* leaves examining the interaction strength of MAC3B$^{\Delta U\text{-box}}$ with ERF13^{WT}, ERF13^{AAA}, and ERF13^{DDD}. BiFC: bimolecular fluorescence complementation. DAPI: diamidino-phenyl-indole, used as a nucleus marker. More than 35 cells were used to quantify signal strength. Student's *t*-test; **, $P<0.01$. **(D)** LCI experiments in *N. benthamiana* leaves examining the interactions of MAC3A$^{\Delta U\text{-box}}$ and MAC3B$^{\Delta U\text{-box}}$ with ERF13^{WT}, ERF13^{AAA}, and ERF13^{DDD}. The color scale from dark blue to yellow reflects the intensity of protein interaction from weak to strong. Bar, 1 cm. **(E)** Degradation rates of GST-ERF13^{AAA}, GST-ERF13^{WT}, and GST-ERF13^{DDD} in cell-free assays using protein extracts from WT and *mac3a mac3b* plants treated with or without NAA. Recombinant purified GST-ERF13^{AAA}, GST-ERF13^{WT}, and GST-ERF13^{DDD} were added to the protein extracts with or without 10 μM NAA and incubated for 15, 30, or 60 min. Protein abundance was determined by probing with anti-GST antibody. Similar results were obtained from three independent experiments, whose averages are indicated below the figure. Each figure panel displays a representative image obtained from a gel-based assay. NAA: naphthaleneacetic acid.

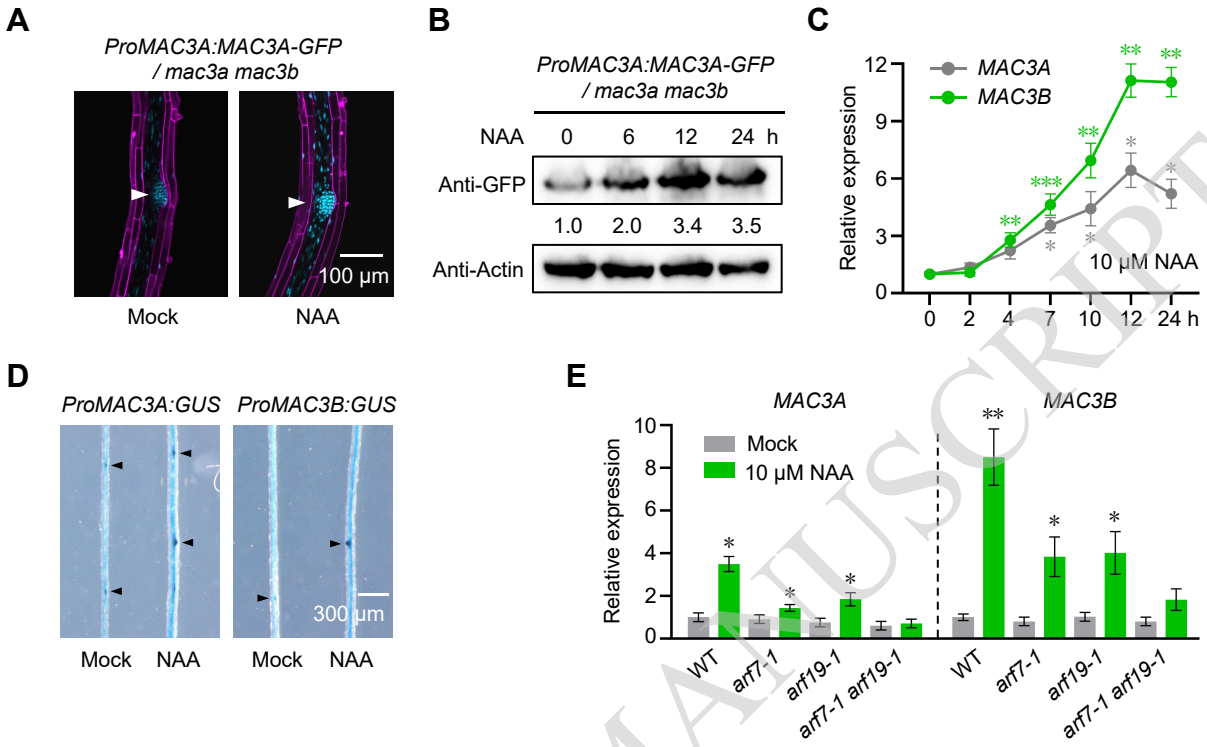

Figure 7. Auxin induces *MAC3A* and *MAC3B* transcription.
(A) Fluorescence images of the LRP of 8-day-old *ProMAC3A:MAC3A-GFP/mac3a mac3b* seedlings treated with or without 10 μM NAA for 10 h. In these fluorescent images, we replaced green (MAC3A-GFP signal) with bright blue and red (propidium iodide signal) with magenta. Arrowheads indicate the lateral root primordia. NAA: naphthaleneacetic acid. GFP: green fluorescent protein. Bar, 100 μm. **(B)** MAC3A-GFP levels in 8-day-old *ProMAC3A:MAC3A-GFP/mac3a mac3b* seedlings treated with 10 μM NAA for the indicated times. Similar results were obtained from three independent experiments, whose averages are indicated below the figure. Each figure panel displays a representative image obtained from a gel-based assay. **(C)** *MAC3A* and *MAC3B* transcript levels in the roots of 8-day-old WT seedlings treated with 10 μM NAA for the indicated times. Three independent biological replicates produced similar results. All time points were compared with the control (0 h). Student's *t*-test; *, $P<0.05$; **, $P<0.01$; ***, $P<0.001$. **(D)** GUS staining images of the roots of 8-day-old *ProMAC3A:GUS* and *ProMAC3B:GUS* seedlings treated with or without 10 μM NAA for 10 h. Arrowheads indicate the lateral root primordia. GUS: histochemical β-glucuronidase. Bar, 300 μm. **(E)** MAC3A and MAC3B transcript levels in the roots of 8-day-old WT, *arf7-1*, *arf19-1*, and *arf7-1 arf19-1* seedlings treated with or without 10 μM NAA for 10 h. Three independent biological replicates produced similar results. Student's *t*-test; *, $P<0.05$; **, $P<0.01$.

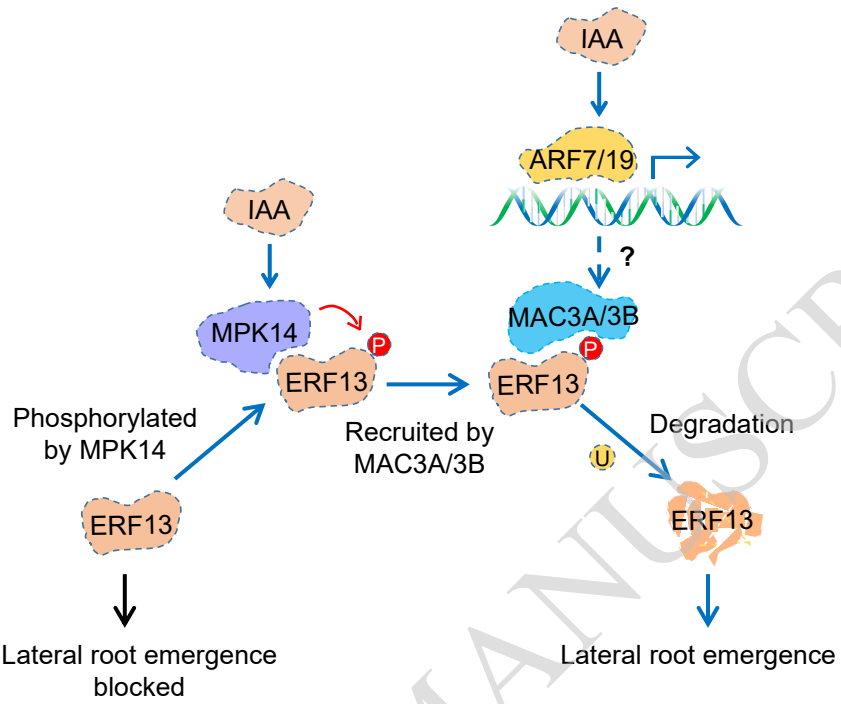

Figure 8. MAC3A and MAC3B mediate auxin signaling to regulate LR emergence via the degradation of ERF13.

At low auxin concentrations, ERF13 acts as a barrier to prevent LR emergence, thereby ensuring that LR development is silenced when auxin levels are insufficient. At high auxin (IAA) concentrations, MPK14 phosphorylates ERF13. Phosphorylated ERF13 preferentially associates with the E3 ligases MAC3A and MAC3B. Moreover, high auxin concentrations promote MAC3A and MAC3B accumulation, a process indirectly mediated by ARF7 and ARF19. MAC3A and MAC3B trigger ERF13 ubiquitination and degradation, ultimately relieving the inhibition of LR emergence. The black line represents the inhibition of LR emergence by ERF13 in the absence of auxin, the blue lines represent the process by which auxin triggers ERF13 degradation, and the red line represents MPK14-mediated phosphorylation of ERF13. The dashed blue lines indicate that the transcriptional activation of *MAC3A* and *MAC3B* by ARF7 and ARF19 is indirect. LR: lateral root. P: phosphorylation. U: ubiquitination. IAA: indoleacetic acid.